Received: 19 January 2021 | Revised: 27 April 2021 | Accepted: 7 July 2021

DOI: 10.1049/mna2.12088

Micro & Nano Letters

The Institution of Engineering and Technology WILEY

ORIGINAL RESEARCH PAPER

Au-TiO_2-ZnO sandwich-structured composite films with enhanced ultraviolet-light photocatalytic activity

Aoqun Jian[1,2] | Wanghao Li[1,2] | Meiling Wang[1,2] | Huaping Jia[1,2] | Shengbo Sang[1,2]

[1] MicroNano System Research Center, College of Information and Computer, Taiyuan University of Technology, Taiyuan, China

[2] Key Laboratory of Advanced Transducers and Intelligent Control System, Taiyuan University of Technology, Taiyuan, China

Correspondence
Shengbo Sang, MicroNano System Research Center, College of Information and Computer, Taiyuan University of Technology, Taiyuan 030024, China.
Email: sunboa-sang@tyut.edu.cn

Funding information
National Natural Science Foundation of China, Grant/Award Number: 61971301, 51622507; 863 project, Grant/Award Number: 2015AA042601; Excellent Talents Technology Innovation Program of Shanxi Province, Grant/Award Number: 201805D211021

Abstract

The rapid recombination of photogenerated electron-hole pairs is one of the main reasons for limiting the photocatalytic efficiency of semiconductor photocatalysts. This paper investigates and analyzes two methods to improve the separation and lifetimes of electron-hole pairs: semiconductor heterojunction and metal electron sink. As a specific example, an Au-TiO_2-ZnO composite film with a sandwich structure is prepared. The energy level gradient formed at the TiO_2/ZnO heterojunction separates the electron-hole pairs effectively, and the AuNPs promote the photo-induced charge transfer. Moreover, a synergistic effect of TiO_2/ZnO heterojunction and AuNPs, which can further improve the photocatalytic performance, has been found by the photoelectric performance measurement. The experimental results demonstrate that the UV photocurrent density of the Au-TiO_2-ZnO composite film is almost 22 times that of the pure TiO_2 film. And a similar result has been observed in the UV light degradation of methylene blue. Such Au-TiO_2-ZnO composite film combining semiconductor heterojunctions and metal electron sink has a potential prospect in the photo-degradation of organic pollutants.

1 | INTRODUCTION

Nowadays, the increasing recalcitrant organic pollutants in air and wastewater have caused serious consequences to people's daily lives and have become a significant global challenge [1–3]. Semiconductor photocatalysts, which can convert light energy into chemical energy with a highly efficient energy conversion coefficient, have been widely utilized in the fields of organic pollutant degradation and harmful gas purification [4–7]. However, the competition between charge recombination and interfacial charge transfer between semiconductors and adsorbates appears to restrict the upper limit of the photocatalytic reaction efficiency of semiconductor photocatalysts [8, 9]. Effective electrons and holes separation and fast charge carrier transport are effective ways to enhance the photocatalytic efficiency of the semiconductor.

The heterojunction structure, composed of two or more different semiconductors, is one of the effective methods to restrain the recombination of photogenerated electron-hole pairs [10, 11]. Due to the difference in energy bandgap positions of semiconductors, an energy gradient can be formed at the interface across the heterojunction, and the driving force produced by the built-in potential effectively accelerates the spatial separation of electrons and holes, and therefore enhances the efficiency of the photocatalytic process [12, 13]. Based on this principle, several sets of combinations of semiconductors, such as SnO_2/ZnO [14], ZnO/TiO_2 [15], WO_3/TiO_2 [8], SnO_2/ZnO/TiO_2 [12], have received widespread attention and are intensively investigated.

On the other hand, the combination of semiconductors with noble metal nanoparticles (NPs) (e.g. Au, Pt, Ag, Pd) can lead to interfacial charge transfer and separation, thus decreasing charge recombination rates and extending the lifetime of the photogenerated electron-hole pairs [15, 16]. During the initial stage of UV illumination, more photogenerated electrons are excited into the conduction band (CB) of the semiconductor, and the Fermi level of the semiconductor lifts. Due to the difference in Fermi level, the photo-excited electrons in the

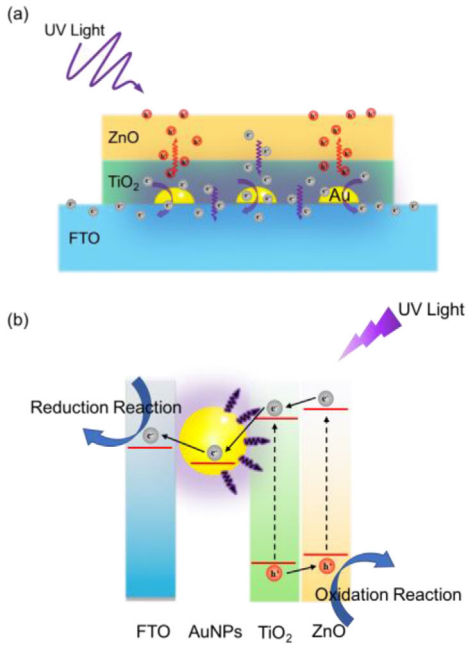

FIGURE 1 (a) The schematic structure of the Au-TiO_2-ZnO composite film; (b) schematic representation of the mechanism of photogenerated charge separation of the Au-TiO_2-ZnO composite film with their corresponding energy band diagrams

semiconductor are driven into the metal particles, which raises the Fermi level of the metal towards the semiconductor CB. The Fermi levels of semiconductor and metal re-equilibrate finally [17, 18]. Except for the electron transfer mechanism, another physical mechanism, intensive far-field light scattering [19], is also beneficial for photocatalytic activity [20, 21].

The above-mentioned two methods of improving the photocatalytic efficiency of semiconductors have been reported in many works. However, for the two methods, their combinational effects and quantitative analysis have been seldom explored. Therefore, in this paper, a composite sandwich-structured Au-TiO_2-ZnO film is proposed of which the schematic structure graph is shown in Figure 1a. The AuNPs, the TiO_2 film, and the ZnO film were sequentially deposited on the fluorine doped tin oxide (FTO) substrate. And the blank area left on the FTO glass around the deposited composite film is designed to migrate electrons to the reaction solution and then participate in reduction reactions.

Although typical powder photocatalysts can fully contact the reactants and have high photocatalytic efficiency, they also suffer from the drawbacks of uneven illumination and difficulty in separating from the reactants [22, 23]. Although the separation issue can be solved by magnetic composite catalysts [24, 25], their complicated preparation process increases cost and hinders their further commercial applications. On the other hand, thin-film, fabricated by the simple spin-coating process, is one of the effective solutions for the separation and recycling of nanomaterials[23]. In addition, rapid reaction speed, low reagent consumption, easy control of flow rates, as well as uniform illumination of light are the unique advantages of the combined application of thin-film photocatalysts and microfluidic reactors [26–29].

The proposed photocatalytic reaction mechanism of the Au-TiO_2-ZnO composite film is shown in Figure 1b. As the CB of ZnO is slightly higher than that of TiO_2 (see Section 3.1 for details) [12, 15, 30], an energy level gradient formed at the interface of ZnO and TiO_2 will separate the photogenerated electron-hole pairs [13, 15]. When the composite film is exposed to the UV light irradiation, the photogenerated electrons in the ZnO will enter the CB of TiO_2, owing to the driving force produced by the built-in potential originating from the heterojunction between TiO_2 and ZnO. Since the Fermi level of AuNPs is much lower than that of TiO_2, the photogenerated electrons in TiO_2 will enter AuNPs along with the electrons that flow from ZnO to TiO_2. Finally, the flowed electrons in AuNPs are transferred into the blank area of the FTO substrate for the reduction reaction. On the other hand, the holes will converge to ZnO for the oxidation reaction [31–33]. AuNPs serve as an electron sink for CB electrons generated in semiconductors, thereby enhancing electron-hole pairs' separation and lifetimes. Such metal electron sink mechanisms, together with the scattering effect, are all beneficial for the catalytic activity.

2 | EXPERIMENTAL SECTION

2.1 | Reagents

Ethanolamine ($HOCH_2CH_2NH_2$, 99%), tetrabutyl titanate ($C_{16}H_{36}O_4Ti$, Tetra-butyl ortho-titanate (TBOT), 98%), Tween 20, diethanolamine ($HN(CH_2CH_2OH)_2$, 99%), 1-Butanol ($CH_3(CH_2)_2CH_2OH$, 99.5%), zinc acetate dihydrate ($(CH_3COO)_2$ $Zn{\cdot}2H_2O$, 99%), ethyl alcohol absolute (C_2H_5OH, 99.7%), and deionized water were used for all the experiments.

2.2 | Preparation of ZnO sol-gel solutions

In this paper, the ZnO and TiO_2 nanofilms were prepared via the sol-gel process. The ZnO sol-gel solutions were prepared as follows. First, 2.1951 g of zinc acetate dihydrate was dissolved in 50 ml of ethanol and stirred for 1 h at 50°C in a water bath to get a precursor solution. Subsequently, 0.6 ml of ethanolamine was added to the precursor at a speed of one drop per second under vigorous stirring. After that, the solution was continuously sonicated for 30 min to achieve a transparent alkaline ZnO sol. Finally, the sol was aged for 24 h for further application [34–36].

2.3 | Preparation of TiO_2 sol-gel solutions

The TBOT was used as a precursor and the TiO_2 sol-gel solutions were prepared at room temperature as follows. First, 24 ml of 1-Butanol, 8.5 ml of TBOT, and 2.4 ml of diethanolamine were mixed and stirred for an hour to get a precursor solution. A mixture of 0.9 ml of deionized water, 12.5 ml of 1-Butanol, and 2 ml of Tween 20 was subsequently dropped into the precursor

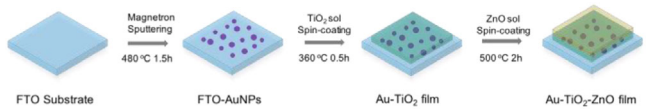

FIGURE 2 Fabrication process of the Au-TiO_2-ZnO composite film

at a speed of one drop per second under vigorous stirring. After that, the solution was continuously stirred for 2 h and achieved a yellow transparent sol. Finally, the sol was aged for 24 h to get an alkaline TiO_2 sol for further application [34–36].

2.4 | Preparation of Au-TiO_2-ZnO composite film

The Au-TiO_2-ZnO composite films were prepared by sequentially depositing the AuNPs, the TiO_2 sol, and the ZnO sol. The procedures are illustrated in Figure 2. Before fabrication, FTO glasses (20 × 20 × 2.2 mm) were cleaned with acetone, ethanol, and deionized water, successively, in an ultrasonic bath for 10 mins. Before each step in the process of preparation of the composite film, apply a thin tape around the conductive surface of the FTO glass to leave a blank area, and tear it off before calcination to avoid contamination of the film. The dried substrates were transferred to a magnetron sputtering system (TRP-450; Sky Technology Development) to deposit a 3nm thick Au layer onto the surface of the FTO glass. Then the samples were annealed at 480°C for 1.5 h to form the AuNPs on the FTO surface. Subsequently, the prepared TiO_2 and ZnO sol were successively coated onto the AuNPs surface via the spin-coating method at a speed of 4000 r/s. After annealing at 360°C for 30 min, the coating operation was carried out once again. The coated samples were then annealed at 500°C for 2 h (Please refer to the appendix Figure S1 for the selection of annealing temperature). The temperature increase during this process was kept at a speed of 2°C/min. After anneal processing, the samples were naturally cooled.

2.5 | Photocatalytic degradation experiment

The photocatalytic degradation performance of Au-TiO_2-ZnO composite film was used with Methylene blue (MB, concentration 1 mM) as a simulated organic pollutant and investigated under a xenon lamp (HSX-F/UV 300, 300< λ <1100 nm) fixed with an ultraviolet reflector (UVREF, 200–400 nm) as a simulated UV light [22, 37]. Before photodegradation, the composite film was placed for 3 h in a dark environment to establish an adsorption-desorption equilibrium. And the circulating water cooling system was utilized to maintain the temperature stability of the catalytic system during the catalytic process. During the experiment, the concentration of the MB solution was recorded with a UV-vis spectrophotometer every 1.5 h. The degradation rate of MB can be measured by monitoring the concentration change of MB at a wavelength of 662 nm using a UV–vis spectrophotometer (U-3900; HITACHI).

2.6 | Characterization

The morphology of the synthesized sample was investigated using a scanning electron microscope (SEM, GeminiSEM 300; ZEISS), energy dispersive spectroscopy (EDS) and atomic force microscopy (AFM, Park systems NX10). The phase purity of the samples was recorded by X-ray diffraction (XRD, SmartLab 9 kW; Rigaku) within a 2θ range from 20° to 80° by using a Cu Kα radiation. The X-ray photoelectron spectroscopy (XPS, EscaLab 250Xi; Thermo Fisher Scientific) was performed to determine the chemical status of the as-prepared Au-TiO_2-ZnO composite film. The ultraviolet photoelectron spectrometer (UPS, EscaLab 250Xi; Thermo Fisher Scientific) was performed to determine the position of the valence band of the prepared TiO_2 and ZnO films. The UV-vis absorption spectra of the samples were retrieved from a UV-vis spectrophotometer (UV-2600; Shimadzu) in the range of 300 to 800 nm. Time-resolved photoluminescence spectra (TRPL) were recorded on a fluorescence spectrometer (FLS 980-STM; Edinburgh instruments). The photocurrent experiments were carried out in an electrochemical station (CS2350H; Corrtest) under the irradiation of a Xenon lamp (UV light illumination, 300 mW/cm^2), and the three-electrode system was immersed in 0.5 M Na_2SO_4, in which the sample was prepared on an FTO glass as a working electrode, a platinum plate as a counter electrode, and a saturated calomel electrode as a reference electrode to evaluate photoelectric properties.

3 | RESULTS AND DISCUSSION

3.1 | Material characterization

A typical scanning electron micrograph of prepared AuNPs on the FTO substrate is shown in Figure 3a. The SEM image demonstrates many small AuNPs are distributed on the large bumps, which are attributable to the rough morphology of the FTO substrate (a root mean square roughness (RMS) of about 32 nm, see appendix Figure S2). The statistics of AuNPs size are mostly in the range of 30–50 nm. Figure 3b is the across section SEM morphology of the Au-TiO_2-ZnO composite film on the FTO substrate. A composite film can be observed on the FTO substrate, whose thickness is approximately 650 nm according to the insert close-up image. And the thickness of the prepared Au-TiO_2-ZnO composite film (around 300 nm) can be obtained by considering the thickness of the SnO_2 film of the FTO substrate (about 350 nm, Figure S2 in the appendix). Based on Figure 3c, the Au-TiO_2-ZnO composite film has a relatively smooth surface, and is uniformly distributed on the surface of the FTO substrate. Additionally, the test results of the EDS spectra of the Au-TiO_2-ZnO composite film demonstrate the existence of Ti, Zn, Au, O, and Sn elements in the composite film.

Figure 4 shows the crystal structure of the FTO substrate, the pure TiO_2 film, the TiO_2-ZnO film and the Au-TiO_2-ZnO film by XRD patterns. From the black curve in Figure 4, it is very obvious that four diffraction peaks representing the FTO

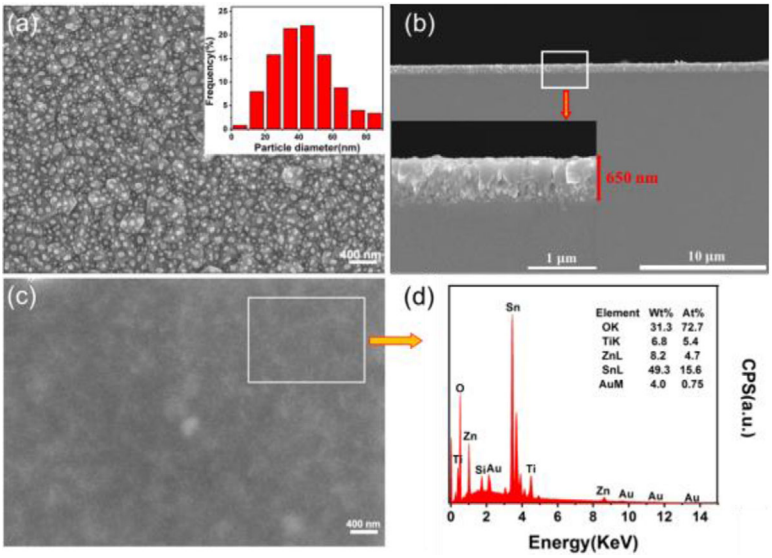

FIGURE 3 (a) Scanning electron micrograph of AuNPs on FTO substrate and statistics of AuNPs size; (b) the across section SEM images of the Au-TiO_2-ZnO composite film on FTO substrate; (c)–(d) the SEM image and the EDS spectrum of the Au-TiO_2-ZnO composite film on the FTO substrate

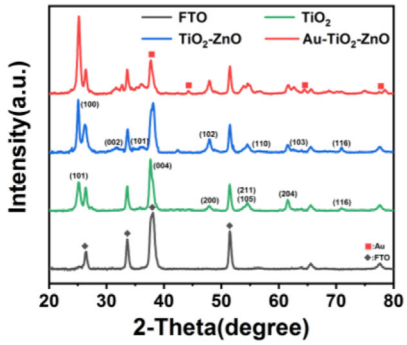

FIGURE 4 XRD patterns of the FTO substrate; the pure TiO_2 film; the TiO_2-ZnO film and the Au-TiO_2-ZnO film

substrate are observed. With the introduction of TiO_2 film (green curve) and ZnO film (blue curve), seven reflection peaks for the TiO_2 can be perfectly indexed as the anatase TiO_2, which have been identified at angles of 25.35°, 37.78°, 48.07°, 53.92°, 55.11°, 62.72° and 68.594° corresponding to (101), (004), (200), (105), (211), (204) and (116), respectively (JCPDS no. 04–0477) [22]; the main diffraction peaks at $2\theta = 31.77°$, 34.42°, 36.25°, 47.54°, 56.60°, 62.86°, 69.09° well match the (100), (002), (101), (102), (110), (103) and (201) planes of the ZnO (JCPDS no. 65–4311) [38]. The XRD spectrum of the Au-TiO_2-ZnO composite film (red curve) not only has the diffraction peaks of TiO_2 and ZnO described above, but also contains the crystal planes of Au ($2\theta = 38.05°$, 44.39°, 64.58°, and 77.56°) [39].

To further investigate the chemical composition of the Au-TiO_2-ZnO composite film, XPS analysis was performed. Due to the depth limitation of the XPS test, the AuNPs, ZnO, and TiO_2 films were tested, respectively. The survey XPS spectrum of TiO_2 is shown in Figure 5a. The Ti 2p spectrum exhibits two peaks, located at 458.5 and 464.2 eV, which can be attributed to the doublet of Ti 2p 3/2 and Ti 2p 1/2, respectively (resulting from the spin-orbit splitting) [33, 40]. Two peaks at 1021.9 and 1045.2 eV are presented in Figure 5b, which are consistent well with the Zn 2p 3/2 and Zn 2p 1/2 corresponding to the chemical element state of Zn^{2+} (ZnO), respectively [41, 42]. As observed in Figure 5c, the peak centred at 529.4 eV corresponds to the Ti–O (lattice O), and another one centred at 531.2 eV is assigned to ZnO (lattice O) [43]. The clear XPS peaks of AuNPs also further reveal the existence of plasmatic Au in the Au-TiO_2-ZnO composite film (see in Figure 5d). The peaks at 83.4 and 87.3 eV are in good agreement with the reported data of Au 4f 7/2 and Au 4f 5/2 [33]. As a result, the above XPS results confirm the coexistence of TiO_2, ZnO, and AuNPs.

As the electric field force for the transfer of electron-hole pairs is closely related to the band structure of the semiconductor in the composite film. Therefore, an UPS was performed to determine the positions of the valence band of the prepared TiO_2 film and ZnO film (shown in Figure 6a,b), which can be calculated by formula $VBM = \hbar\upsilon - (Ek_{max} - Ek_{min})$. The excitation photon energy $\hbar\upsilon$ of the He I lamp is 21.22 eV, Ek_{max} is the Fermi edge, and Ek_{min} is the SE cutoff edge [44, 45]. Therefore, the valence band positions of TiO_2 and ZnO are 7.41 and 7.39 eV respectively [31]. As the valence band position of ZnO is higher than that of TiO_2, while the bandgap of ZnO and TiO_2 are both about 3.2 eV, so the CB energy level of ZnO is slightly higher than that of TiO_2.

After obtaining the valence band positions of the prepared TiO_2 and ZnO, in order to better determine the band structure of the Au-TiO_2-ZnO composite film, it is also necessary to determine the bandgap width of the prepared TiO_2 and ZnO. According to the absorption spectra of the pure TiO_2 and ZnO films (Figure 6c) (see appendix Figure S3 for the absorption of other composite films), the bandgap energy of TiO_2 and ZnO can be derived from the relationship between light energy $(\alpha\hbar\nu)^2$ and photon energy $\hbar\nu$ (Figure 6d). The band gap energies of the prepared TiO_2 and ZnO are calculated to be 3.66 and 3.74 eV, respectively, and the difference between them is 0.08 eV. Based on the UPS test results (the valence band positions of TiO_2 and ZnO are 7.41 and 7.39 eV, respectively), the band structure of the Au-TiO_2-ZnO composite film can be obtained

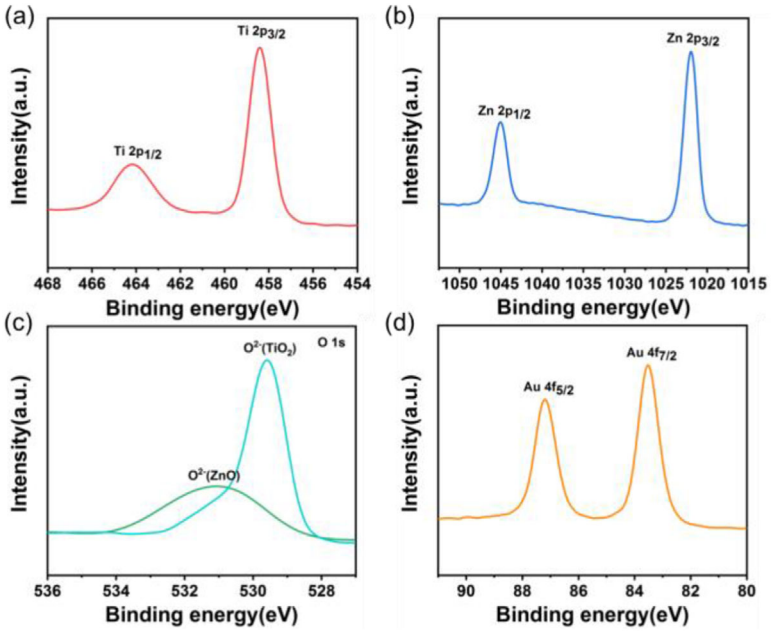

FIGURE 5 XPS spectra (a) Ti 2p; (b) Zn 2p; (c) O 1s; (d) Au 4f

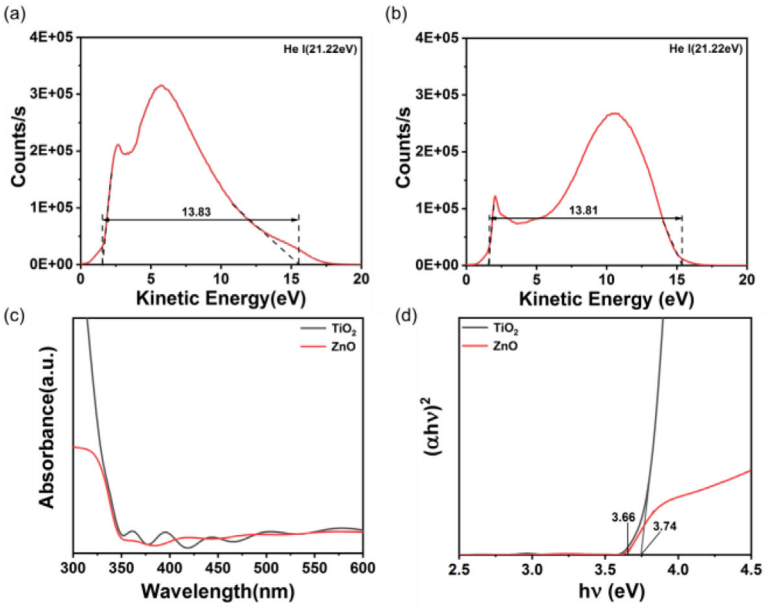

FIGURE 6 UPS spectra of (a) TiO_2 and (b) ZnO; (c) UV-vis absorption spectra of the bare TiO_2 film and the bare ZnO film; (d) Tauc plots calculated from c

as shown in Figure 1b [15, 31]. The energy gradient formed at the TiO_2/ZnO interface facilitates the electrons generated in ZnO to enter the CB of TiO_2. On the contrary, the holes of TiO_2 are driven to enter the VB of ZnO, thereby the separation and lifetime of electron-hole pairs are enhanced effectively [12, 15].

3.2 | Electrochemical characterization

To verify the improved photoelectric properties of the Au-ZnO-TiO_2 film, the photoelectrochemical properties of different composite films were investigated. Under ultraviolet irradiation, the linear sweep voltammograms curves and photocurrent response curves of the bare TiO_2 film, the Au-TiO_2, the TiO_2-ZnO film and the Au-TiO_2-ZnO film, are represented in Figure 7a,b. It should be noted that, in order to ensure the measurements are taken under the same experimental condition, all the films involved in the measurement share the same thickness in the following experiments. As shown in Figure 7a, compared with the current density measured under dark scanning (0.013 mA/cm^2, at a bias voltage of 0.5 V, as the background current) (the current density of all films was roughly consistent under dark scanning, thereby, taking the scanning results of the Au-TiO_2-ZnO film as an example), the current densities of all the composite films show pronounced values under UV light irradiation. Comparing with the current difference between the light and dark environments

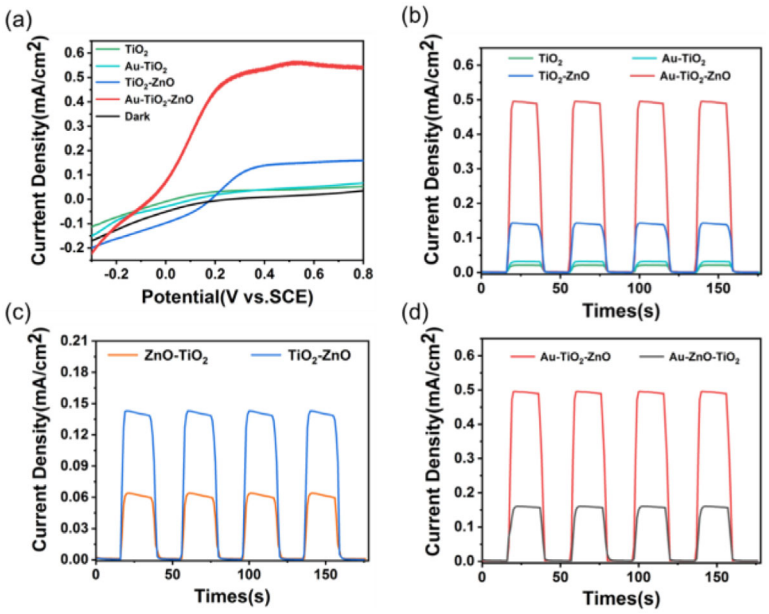

FIGURE 7 Under UV light, the bare TiO_2 film, the Au-TiO_2 film, the TiO_2-ZnO film and the Au-TiO_2-ZnO film, all are on the FTO substrate. (a) LSV curves; (b) photocurrent response curves; (c) photocurrent response curves of the ZnO-TiO_2 film and the Au-TiO_2-ZnO film; (d) Photocurrent response curves of the Au-ZnO-TiO_2 film and the Au-TiO_2-ZnO film

at the same voltage, this experiment selected a bias voltage of 0.5 V as the photoanode bias voltage for the following experiments.

In Figure 7b, the bare TiO_2 film has the lowest photocurrent density values (0.022 mA/cm^2) among all the samples. The Au-TiO_2 film presents an increased photocurrent density (0.034 mA/cm^2, about 1.5 times compared with TiO_2 films), which indicates that AuNPs serve as an electron sink for CB electrons generated in TiO_2 and thus promote the separation of electron-hole pairs. Besides, the TiO_2-ZnO film shows a higher photocurrent density of 0.14 mA/cm^2, about 6.5 times compared with the bare TiO_2 film, which can be attributed to the TiO_2/ZnO heterojunction that effectively enhances the separation and lifetime of electron-hole pairs. It can be found that the enhancement in photocurrent density of TiO_2-ZnO film is much higher than that of Au-TiO_2 film, which indicates that the heterojunction has a stronger effect on electron-hole pair separation in comparison with the AuNPs. Moreover, the Au-TiO_2-ZnO composite films exhibit the strongest photocurrent response under UV illumination, which is 22, 15 and 3.5 times as large as that of the bare TiO_2 film, the Au-TiO_2, and the ZnO-TiO_2 film, respectively.

Based on the above experimental results, if the influence of the AuNPs on the photoelectric performance of thin films is analyzed in-depth, the four sets of data can be divided into two comparative groups. That is, compared with TiO_2 and Au-TiO_2 (1.5 times difference), the difference in photocurrent density between TiO_2-ZnO and Au-TiO_2-ZnO is 3.5 times. The change between these two groups lies in the presence of TiO_2/ZnO heterojunction. It is found that the comparison of TiO_2-ZnO and Au-TiO_2-ZnO, which both have the TiO_2/ZnO heterojunction, exhibits more significant improvement (3.5 times vs. 1.5 times). This amazing result indicates that a synergistic effect between the TiO_2/ZnO heterojunction and the AuNPs has been generated. It can be concluded that, under ultraviolet light irradiation, the photogenerated electrons in ZnO and TiO_2 are converged in the CB of TiO_2 under the driving force produced by the built-in potential based on the TiO_2/ZnO heterojunction. As an electron collector, the AuNPs transport the flowing electrons in the CB of TiO_2, which prevents the built-in electric field from entering into an equilibrium state, thus the transfer of more electrons can be achieved.

Figure 7c,d present the measured photocurrent curves of the four composite films with shifted ZnO and TiO_2 deposition sequences (ZnO-TiO_2 and TiO_2-ZnO films, Au-ZnO-TiO_2 and Au-TiO_2-ZnO films). It can be seen that the photocurrent density of the TiO_2-ZnO film (blue curve) is 2.2 times that of the ZnO-TiO_2 film (orange curve) (0.145 vs. 0.065 mA/cm^2), and the photocurrent density of the Au-TiO_2-ZnO film (red curve) is about 3.2 times that of the Au-ZnO-TiO_2 film (black curve) (0.5 vs. 0.155 mA/cm^2). These experimental results are consistent well with the theoretical analysis of the TiO_2/ZnO heterojunction. According to the energy level positions of ZnO and TiO_2, the composite film, which takes the ZnO film as the outermost layer (TiO_2-ZnO and Au-TiO_2-ZnO films), can conduct more electrons to the FTO substrate by TiO_2/ZnO heterojunction. Taking the control experiment in Figure 7d as an example, the electrons in the Au-TiO_2-ZnO film are collected in AuNPs with the same movement direction. However, for Au-ZnO-TiO_2 film, part of the electrons in ZnO will transfer to TiO_2, where the heterojunction has a negative effect. Therefore, the photocurrent density of the former is much higher than that of the latter.

Moreover, comparing the two groups of experiments in Figure 7c,d, it can be found that the difference between the two comparative experiments is whether the prepared thin film contained AuNPs, and the comparison contained AuNPs (Au-ZnO-TiO_2 film vs. Au-TiO_2-ZnO film) shows greater improvement (2.2 times vs. 3.2 times). This result once again proves that there is a synergistic effect between the TiO_2/ZnO heterojunction and the AuNPs, which makes the positive effect of the TiO_2/ZnO heterojunction amplified.

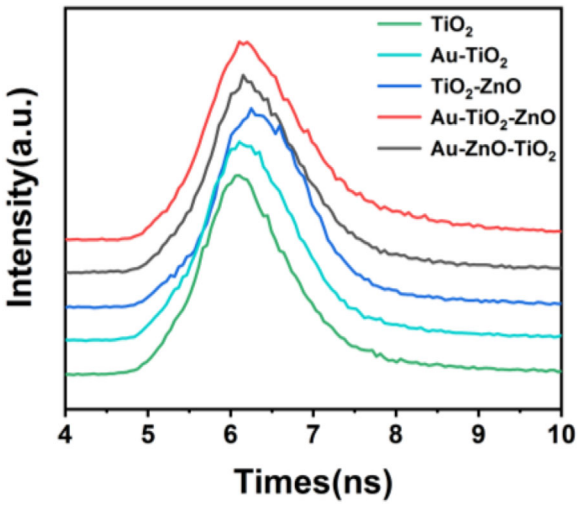

FIGURE 8 Time-resolved fluorescence spectra of the bare TiO_2 film, the Au-TiO_2 film, the TiO_2-ZnO film, the Au-TiO_2-ZnO film and the Au-ZnO-TiO_2 film, all are on the FTO substrate

TABLE 1 Fitting results of time-resolved fluorescence spectra

Sample	τ_1 (ns)	A_1 (%)	τ_2 (ns)	A_2 (%)	τ_{ave} (ns)
TiO_2	0.62	81.48	3.35	18.52	1.13
Au-TiO_2	0.62	84.46	4.14	15.54	1.16
TiO_2-ZnO	0.65	83.52	4.33	16.48	1.26
Au-TiO_2-ZnO	0.8	73.55	4.37	26.45	1.74
Au-ZnO-TiO_2	0.69	83.99	5.98	16.01	1.53

In order to further verify the conclusions drawn from the photocurrent response, TRPL measurements are concluded at room temperature, as shown in Figure 8 and Table 1. After curve-fitting all the measurement results with an exponential model, the pure TiO_2 film and the Au-TiO_2 film have the shortest decay time ($\tau_1 = 0.62$ ns). With the introduction of ZnO thin film, the enhanced decay time can be attributed to the intensified separation of photo-generated electron-hole pairs, which originates from the heterojunction between ZnO and TiO_2. In addition, the Au-TiO_2-ZnO composite film showed the longest decay time ($\tau_1 = 0.8$ ns) in all samples, which can be attributed to the ZnO/TiO_2 heterojunction and the Schottky heterojunction between Au/TiO_2. The energy gradient formed between the ZnO/TiO_2 heterojunctions can effectively separate the photogenerated electron-hole pairs, and Au nanoparticles accelerate the transfer of electrons. The test results of TRPL are completely consistent with the photocurrent response experiment performed above.

3.3 | Photodegradation performance

The MB solution (methylene blue, concentration 1 mM) was degraded under the UV light irradiation to evaluate the photocatalytic performance of the prepared samples: the bare TiO_2, the Au-TiO_2, TiO_2-ZnO and Au-TiO_2-ZnO films, the FTO substrate (no catalysts) as the contrast. As shown in Figure 9a, among these four composite films, Au-TiO_2-ZnO composite film has the highest photocatalytic activity with a degradation rate of 96.0% after 10.5 h. Its degradation efficiency at 10.5 h is 3.8 times, 2.7 times and 1.6 times as those of the bare TiO_2, the Au-TiO_2, and the TiO_2-ZnO films, respectively. It is clear that the experimental results of UV degradation of MB solution are similar to electrochemical test results. The photogenerated electrons, separated by TiO_2-ZnO heterojunctions and AuNPs, assembled on the blank area of the FTO glass substrate to participate in the reduction reaction.

To investigate the reusability and stability of the composite film, the MB photocatalytic degradation experiment of the Au-TiO_2-ZnO composite film was repeated 5 times (as shown in Figure 9b). The degradation efficiency remains stable after five consecutive recycles, and almost achieves high degradation of 85%, confirming the strong stability of the Au-TiO_2-ZnO composite film.

4 | CONCLUSION

In summary, the Au-TiO_2-ZnO composite film was successfully prepared by the magnetron sputtering and spin coating method. The structure and chemical state of the composite photocatalyst are confirmed by various characterizations. Two main mechanisms for enhancing photocatalytic performance are experimentally demonstrated by photoelectric performance characterization: TiO_2/ZnO heterojunction facilitates the separation of electrons and holes, and AuNPs serve as an electron sink to improve the electron conduction properties, and the synergism between TiO_2/ZnO heterojunction and AuNPs has been

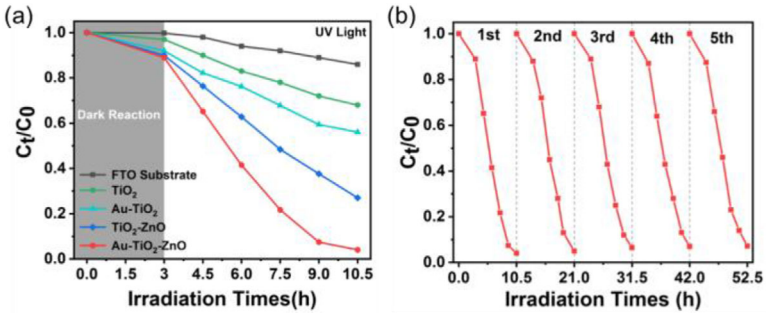

FIGURE 9 (a) Photocatalytic degradation of MB in the presence of different film: the bare TiO_2, Au-TiO_2, TiO_2-ZnO and Au-TiO_2-ZnO films, all are on the FTO substrate, and the FTO substrate (no catalysts) as a comparison, under UV light; (b) performance of repeated test of the Au-TiO_2-ZnO film

found surprisingly. The photocurrent density of the Au-TiO_2-ZnO composite film is almost 22 times that of the pure TiO_2 film with the same thickness. Such Au-TiO_2-ZnO sandwich-structured composite film has the advantages of improved photocatalytic efficiency and strong stability, and brings a new solution for photocatalytic degradation of pollutants.

ACKNOWLEDGEMENTS

This study was financially supported by the National Natural Science Foundation of China (61971301, 51622507), 863 project (2015AA042601), Excellent Talents Technology Innovation Program of Shanxi Province (201805D211021).

DATA AVAILABILITY STATEMENT

The data that supports the findings of this study are available in the supplementary material of this article.

ORCID

Shengbo Sang https://orcid.org/0000-0003-3011-7632

REFERENCES

1. Shi, W., et al.: Nanoporous Pt/TiO_2 nanocomposites with greatly enhanced photocatalytic performance. J. Chin. Chem. Soc. 65(11), 1286–1292 (2018)
2. Liu, C., et al.: Biomimetic synthesis of TiO_2-SiO_2-Ag nanocomposites with enhanced visible-light photocatalytic activity. ACS Appl. Mater. Interfaces 5(9), 3824–3832 (2013)
3. Todorova, N., et al.: Photocatalytic NOx oxidation over modified ZnO/TiO_2 thin films. Catal. Today 252, 41–46 (2015)
4. Khan, M.M., et al.: Metal oxides as photocatalysts. J. Saudi. Chem. Soc. 19(5), 462–464 (2015)
5. Gaya, U.I., Abdullah, A.H.: Heterogeneous photocatalytic degradation of organic contaminants over titanium dioxide: A review of fundamentals, progress and problems. J. Photochem. Photobiol. C Photochem. Rev. 9(1), 1–12 (2008)
6. Fang, J., et al.: Au@TiO_2–CdS ternary nanostructures for efficient visible-light-driven hydrogen generation. ACS Appl. Mater. Interfaces 5(16), 8088–8092 (2013)
7. Fang, J., et al.: A facile way to synthesize cost-effective ZnO nanorods with enhanced photocatalytic activity. Mater. Lett. 120, 147–150 (2014)
8. Luévano-Hipólito, E., et al.: Synthesis, characterization and photocatalytic activity of WO_3/TiO_2 for NO removal under UV and visible light irradiation. Mater. Chem. Phys. 148(1-2), 208–213 (2014)
9. Liu, X., et al.: Porous TiO_2 assembled from monodispersed nanoparticles. Nanoscale Res. Lett. 11(1), 159–167 (2016)
10. Kim, C.-Y., et al.: Open-circuit voltage improvement in InGaAs/InP heterojunction solar cells. Jpn. J. Appl. Phys. 44(4B), 2523–2524 (2005)
11. Ji, S., et al.: A high-performance room-temperature NO_2 sensor based on an ultrathin heterojunction film. Adv. Mater. 25(12), 1755–1760 (2013)
12. Yang, G., et al.: Preparation and characterization of SnO_2/ZnO/TiO_2 composite semiconductor with enhanced photocatalytic activity. Appl. Surf. Sci. 258(22), 8704–8712 (2012)
13. You, H., et al.: High-efficiency and mechano-/photo-bi-catalysis of piezoelectric-ZnO@ photoelectric-TiO_2 core-shell nanofibers for dye decomposition. Chemosphere 183, 528–535 (2017)
14. Wang, C., et al.: Enhanced photocatalytic performance of nanosized coupled ZnO/SnO_2 photocatalysts for methyl orange degradation. J. Photochem. Photobiol. A Chem. 168(1-2), 47–52 (2004)
15. Cheng, C., et al.: Enhanced photocatalytic performance of TiO_2-ZnO hybrid nanostructures. Sci. Rep. 4, 4181–4186 (2014)
16. Sheng, F., et al.: Simulation on field enhanced electron transfer between the interface of ZnO–Ag nanocomposite. J. Phys. Chem. C 117(36), 18627–18633 (2013)
17. Subramanian, V., et al.: Semiconductor-metal composite nanostructures. To what extent do metal nanoparticles improve the photocatalytic activity of TiO_2 films?. J. Phys. Chem. B 105, 11439–11446 (2001)
18. Kamat, P.V.: Photophysical, photochemical and photocatalytic aspects of metal nanoparticles. J. Phys. Chem. B 106, 7729–7744 (2002)
19. Temple, T.L., et al.: Influence of localized surface plasmon excitation in silver nanoparticles on the performance of silicon solar cells. Sol. Energy Mater. Sol. Cells 93(11), 1978–1985 (2009)
20. Wu, N.: Plasmonic metal-semiconductor photocatalysts and photoelectrochemical cells: A review. Nanoscale 10(6), 2679–2696 (2018)
21. Jang, Y.H., et al.: Plasmonic solar cells: From rational design to mechanism overview. Chem. Rev. 116(24), 14982–15034 (2016)
22. Jia, H., et al.: Microfluidic reactors for plasmonic photocatalysis using gold nanoparticles. Micromachines 10(12), 869–880 (2019)
23. Lindstrom, H., et al.: High surface area titania photocatalytic microfluidic reactors. AlChE J. 53(3), 695–702 (2007)
24. Mamba, G., Mishra, A.: Advances in magnetically separable photocatalysts: Smart, recyclable materials for water pollution mitigation. Catalysts 6(6), 79 (2016)
25. Sydnes, M.: The use of palladium on magnetic support as catalyst for Suzuki–Miyaura cross-coupling reactions. Catalysts 7(12), 35 (2017)
26. Liao, W., et al.: Biomimetic microchannels of planar reactors for optimized photocatalytic efficiency of water purification. Biomicrofluidics 10(1), 014123–014132 (2016)
27. Matsushita, Y., et al.: Recent progress on photoreactions in microreactors. Pure Appl. Chem. 79(11), 1959–1968 (2007)
28. Liu, A.L., et al.: Study on the photocatalytic reaction kinetics in a TiO_2 nanoparticles coated microreactor integrated microfluidics device. Talanta 182, 544–548 (2018)
29. Jing, Z., et al.: Highly sensitive, reliable and flexible piezoresistive pressure sensors based on graphene-PDMS @ sponge. J. Micromech. Microeng. 30(8), 085012–085021 (2020)
30. Hernández, S., et al.: Comparison of photocatalytic and transport properties of TiO_2 and ZnO nanostructures for solar-driven water splitting. Phys. Chem. Chem. Phys. 17(12), 7775–7786 (2015)
31. Zhang, X., et al.: Plasmonic photocatalysis. Rep. Prog. Phys. 76(4), 046401–046443 (2013)
32. Xie, H., et al.: Effects of Au nanoparticles and ZnO morphology on the photocatalytic performance of Au doped ZnO/TiO_2 films. Nanotechnology 30(8), 085708–085721 (2019)
33. Hu, S., et al.: Plasmonic Au-TiO_2/ZnO core-shell nanorod array photoanode for visible-light-driven photoelectrochemical water splitting. Energy Technol. 5(9), 1599–1605 (2017)
34. Tian, J., et al.: Preparation and characterization of TiO_2, ZnO, and TiO_2/ZnO nanofilms via sol–gel process. Ceram. Int. 35(6), 2261–2270 (2009)
35. Gaspera, E.D., et al.: Au nanoparticle monolayers covered with sol–gel oxide thin films: Optical and morphological study. Langmuir 27(22), 13739–13747 (2011)
36. Jiang, X., et al.: Enhanced UV emission of TiO_2–ZnO nanocomposite films synthesized by simplified sol–gel dip-coating method. Mater. Express 8(3), 288–293 (2018)
37. Jian, A., et al.: One-pot synthesis of Cu_2O/C@H-TiO_2 nanocomposites with enhanced visible-light photocatalytic activity. RSC Adv. 9(71), 41540–41548 (2019)
38. Misra, M., et al.: Surface plasmon quenched of near band edge emission and enhanced visible photocatalytic activity of Au@ZnO core-shell nanostructure. Appl. Catal. B Environ. 150-151, 605–611 (2014)
39. Huang, J., et al.: Bifunctional Au@TiO_2 core–shell nanoparticle films for clean water generation by photocatalysis and solar evaporation. Energy Convers. Manage. 132, 452–459 (2017)
40. Li, S., et al.: Sandwich-like TiO_2@ZnO-based noble metal (Ag, Au, Pt, or Pd) for better photo-oxidation performance: Synergistic effect between noble metal and metal oxide phases. Appl. Surf. Sci. 443, 603–612 (2018)
41. Do, Y.-J., et al.: The interfacial nature of TiO_2 and ZnO nanoparticles modified by gold nanoparticles. Bull. Korean Chem. Soc. 31(8), 2170–2174 (2010)

42. Chen, Y.-W., et al.: Preferential oxidation of CO in H2 stream on Au/ZnO–TiO_2 catalysts. Int. J. Hydrogen Energy 37(20), 15140–15155 (2012)
43. Zhang, P., et al.: In situ assembly of well-dispersed Au nanoparticles on TiO_2/ZnO nanofibers: A three-way synergistic heterostructure with enhanced photocatalytic activity. J. Hazard. Mater. 237–238, 331–338 (2012)
44. Scudiero, L., et al.: Scanning tunneling microscopy, orbital-mediated tunneling spectroscopy, and ultraviolet photoelectron spectroscopy of nickel(II) octaethylporphyrin deposited from vapor. J. Phys. Chem. B 106(5), 996–1003 (2002)
45. Juan Liu, Y.L., et al.: Metal-free efficient photocatalyst for stable visible water splitting via a two-electron pathway. Science 347(6225), 970–974 (2015)
46. Ting, S., et al.: Photocatalytic oxidation of acetone over high thermally stable TiO_2 nanosheets with exposed (001) facets. Front Chem. 6, 175–185 (2018)
47. Long, L., et al.: Enhanced photocatalytic performance of platinized CdS/TiO_2 by optimizing calcination temperature of TiO_2 nanotubes. Mater. Sci. Semicond. Process. 26, 107–111 (2017)
48. Li, X., Zeng, L.: Effect of calcination temperature on photocatalytic activity of ZnO. Foshan Ceramics 21(179), 29–32 (2011)

SUPPORTING INFORMATION

Additional supporting information may be found online in the Supporting Information section at the end of the article.

How to cite this article: Jian, A., et al.: Au-TiO_2-ZnO sandwich-structured composite films with enhanced ultraviolet-light photocatalytic activity. Micro Nano Lett. 16:601–609 (2021).
https://doi.org/10.1049/mna2.12088

APPENDIX

Under UV irradiation, the photocurrent response test results of the TiO_2 and ZnO films with different annealing temperatures (450°C, 500°C and 550°C) are shown in Figure S1a,b. The results show that the TiO_2 and ZnO films annealed at 500°C have the highest photocurrent response, which is consistent with the results of some previous studies [46–48]. For the composite films, on the basis of calcining the inner layer at the optimal temperature, the effect of calcining the outer layer at different temperatures on the overall photocurrent response of the composite film have been tested (Figure S1c, d). In the case of Au-ZnO-TiO_2 film, the ZnO film was calcined at 500°C, while the TiO_2 film was calcined at 450°C, 500°C and 550°C, respectively. The results show that the outer layer TiO_2 calcined at 500°C has the highest photocurrent density. Furthermore, the results show that 500°C is still the best annealing temperature for the Au-TiO_2-ZnO film.

The absorption spectra of the bare TiO_2, the Au-TiO_2, the TiO_2-ZnO, the Au-TiO_2-ZnO and the AuNPs films are presented in Figure S3. All the samples except for the AuNPs film have strong absorption in the ultraviolet region, which is mainly due to the absorption of TiO_2 and ZnO. It can be observed from the Figure S3 that the $TiO_2$and TiO_2-ZnO films only have absorption in the ultraviolet light band. With the introduction of AuNPs, each group of samples has an obvious absorption peak in the visible light band, which can be attributed to the LSPR effect of the AuNPs.

The energy band structure of the FTO/Au/ZnO/TiO_2 structure is shown in Figure S4a. Under ultraviolet light irradiation, both ZnO and TiO_2 are excited to generate electron-hole pairs. On the one hand, due to the existence of ZnO/TiO_2 heterojunction, some electrons in ZnO will enter the CB of TiO_2 along the energy gradient; on the other hand, due to the existence of AuNPs, more electrons generated in ZnO enter Au nanoparticles. In combination with the photocurrent response test results (as shown in Figure S4b), the photocurrent density of the pure ZnO film is 0.078 mA/cm^2, and the increasing photocurrent density (0.095 mA/cm^2) of Au-ZnO can be attributed to the electron conduction of AuNPs. It is not surprising that ZnO-TiO_2 exhibits the smallest photocurrent density (0.065 mA/cm^2), because the heterojunction here has a negative effect on the direction of electron flow.

It has been noted that the Au-ZnO-TiO_2 film has the highest photocurrent density (0.155 mA/cm^2), and the specific analysis is as follows: normally, there is a bending of the energy band at the junction of the semiconductor and the electrolyte surface, although the ZnO/TiO_2 heterojunction makes the electron flow direction is opposite to the overall electron transfer direction, because of the bending of the energy band between the TiO_2 and the electrolyte surface, the electrons cannot be easily introduced into the solution. When the electrons in the TiO_2 accumulate to a certain amount, some electrons will enter the ZnO, so it will lead to an increase in the overall photocurrent density. However, such enhancement is much lower than the synergistic effect of the FTO/Au/ZnO/TiO_2 structure.